

Article

Preparation and Optical Property of Far-Red LED Encapsulated with the Graded-Index Fluorescent Glass Film

Shihong Liang¹, Bin Wang¹, Xiangfu Wang^{1,2,*}  and Xiaohong Yan^{1,3,*}

¹ College of Electronic and Optical Engineering & College of Flexible Electronics (Future Technology), Nanjing University of Posts and Telecommunications, Nanjing 210023, China; 1020020803@njupt.edu.cn (S.L.); 1220024519@njupt.edu.cn (B.W.)

² The State Key Laboratory of Refractories and Metallurgy, Wuhan University of Science and Technology, Wuhan 430065, China

³ The Key Laboratory of Radio and Micro-Nano Electronics of Jiangsu Province, Nanjing 210023, China

* Correspondence: xfwang@njupt.edu.cn (X.W.); yanxh@njupt.edu.cn (X.Y.)

Abstract: Fabricating far-red light-emitting diodes (LEDs) with high emission efficiency is a change for the application in plant growth. In this work, a new type of far-red LED was fabricated for plant growth by encapsulating the $\text{Sr}_3\text{LiSbO}_6:\text{Mn}^{4+}$, Mg^{2+} ($\text{SLSO}:\text{Mn}^{4+}$, Mg^{2+}) far-red phosphors with the gradient-refractive glass films. Under 365 nm excitation, the phosphors emitted the wide band in the 550–800 nm range, which overlapped with the absorption band of plants that absorb far-red light (PFR). The internal quantum efficiency (IQE) of the LED was 93.6%. Compared with the luminous efficacy of traditional (fluorescent silicone) LEDs (59 lm/W), the luminous efficacy of the new LED is increased by 62.7%, and reaches 96.74 lm/W. Thus, this far-red LED with high IQE has a long-term application prospect in plant growth.

Keywords: light-emitting diodes; luminous efficiency; gradient refractive



Citation: Liang, S.; Wang, B.; Wang, X.; Yan, X. Preparation and Optical Property of Far-Red LED Encapsulated with the Graded-Index Fluorescent Glass Film. *Electronics* **2023**, *12*, 3448. <https://doi.org/10.3390/electronics12163448>

Academic Editor: Jiun-Haw Lee

Received: 27 June 2023

Revised: 30 July 2023

Accepted: 9 August 2023

Published: 15 August 2023



Copyright: © 2023 by the authors. Licensee MDPI, Basel, Switzerland. This article is an open access article distributed under the terms and conditions of the Creative Commons Attribution (CC BY) license (<https://creativecommons.org/licenses/by/4.0/>).

1. Introduction

In recent years, the development of green agriculture has become a global concern [1–3]. In the visible band, the absorption capacity of phytochromes that complete photosynthesis is 350–450 nm and 660–720 nm [4,5]. The phytochromes of plants absorb red light (PR) and far-red light (PFR) to jointly regulate the development of plant morphology [6–8]. Therefore, it was found that plants were susceptible to red and far-red light. At present, halogen and incandescent lamps are mainly used in greenhouses, while white LED panel lamps are primarily used in plant factories [9–11]. The spectra of these light sources do not overlap with the photosynthetic spectra of plants, since the traditional LEDs lacked far-red light in the band from red light to far-red light (640–750 nm) [12]. Moreover, the traditional LEDs had the bottleneck of low luminous efficiency, color-rendering index difference, and low thermal stability [13–15]. LEDs exhibit light-emission efficiency through their internal quantum efficiency (IQE), light-extraction efficiency (LEE), and external quantum efficiency (EQE). The higher the IQE, the more photons are emitted, resulting in increased light absorption by plants.

In order to solve these problems, Peng studied the optimal distance between the phosphor layer and the chip to reduce the backscattering of light and enhanced the optical efficiency [16]. Fluorescent glass film was used to increase the thermal stability of LEDs [17]. It was found that the light output efficiency was increased by reducing the backscattering of LEDs [18]. To increase the color temperature, Sang mixed red phosphor $\text{CaAlSiN}_3:\text{Eu}^{2+}$ and yellow phosphor $\text{Y}_3\text{Al}_5\text{O}_{12}:\text{Ce}^{3+}$ into the glass matrix for high-power LEDs, and reduced the color temperature to 3290 K [19]. Cao used the screen-printing method to coat the red phosphor $\text{K}_2\text{SiF}_6:\text{Mn}^{4+}$ onto the $\text{LuAG}:\text{Ce}^{3+}$ yellow phosphor for high-power white LEDs, in which the color temperature is decreased to 3744 K [20]. However, all of these studies

focused on the spectra and conversion efficiency of phosphors and did not consider the influence of physical structure on LEDs. Therefore, it needs to enhance the light-output efficiency of the LEDs by designing a new optical structure.

In this paper, we design a new type of far-red LED with the package of gradient-refractive fluorescent glass, which is suitable for improving the light-absorption rate of plants and realizes the overlap of broadband emission of LEDs and the absorption of plant pigments. Because silicone is not heat-resistant, the life of traditional LEDs is not long [21]. Therefore, the selection of heat-resistant glass beads instead of silicone is necessary. By designing the package of gradient-refractive fluorescent glass, the light-output efficiency was improved. The IQE of the resulting LED was 93.6%. Compared with traditional LEDs, the luminous efficiency of the new LED reached 96.74 lm/W. Under 365 nm excitation, the new LED emitted the wide band in the 550–800 nm range, which overlapped with the absorption band of PFR. These results indicate that the resulting LEDs are promising for application in plant lighting sources.

2. Materials and Methods

A series of phosphor particles, such as $\text{Sr}_3\text{LiSbO}_6: x\text{Mn}^{4+}, y\text{Mg}^{2+}$ ($x = 0, 0.2\%, 2\%$; $Y = 0, 0.3\%, 2\%$; SLSO), were successfully prepared by a high-temperature solid-state method. High-purity Li_2CO_3 (99.9%), SrCO_3 (A.R), Sb_2O_5 (A.R) and MnCO_3 (99.9%), MgCO_3 (99.9%) as starting materials. Weigh the above materials with the stoichiometric amounts and grind them in alcohol with an agate mortar for 2 h. The mixed powder was calcined in a muffle furnace at $5^\circ\text{C}/\text{min}$ to 1200°C for 6 h. Finally, the sample was cooled to room temperature and ground into powder again.

The $(\text{P}_2\text{O}_5\text{-ZnO-B}_2\text{O}_3\text{-Li}_2\text{CO}_3\text{-BaO})$ glass was prepared by the high-temperature solid-state method. The matrix glass stoichiometric ratio was $(38-x)\text{P}_2\text{O}_5\text{-}45\text{ZnO}\text{-}10\text{B}_2\text{O}_3\text{-}4\text{Li}_2\text{CO}_3\text{-}x\text{BaO}$ ($x = 3, 6, 9$ mol%). P_2O_5 (AR), ZnO (99%), B_2O_3 (98%), and Li_2CO_3 (AR) were used as experimental raw materials. Weigh 10 g of raw materials according to the proportion, put the mixture into the fresh grinding bowl, add alcohol to mix it thoroughly, heat the mixture in the lifting furnace with the speed of $4^\circ\text{C}/\text{min}$ to 1200°C , and heat it for 2 h to melt the raw materials into liquid. Then, pour the glass melt into the preheated copper mold, annealed at 350°C for 50 min, and cooled to room temperature. Grind the prepared glass test data into powder for subsequent experiments.

The ratio of glass powder to phosphor (fluorescent glass powder) is 1:1. The ratio of fluorescent glass powder to the organic solvent is 5:4. The terpeneol (AR), Butyldiglycol (99%), and ethyl cellulose (CP) are organic solvents. Under the 80°C water bath condition, solids and liquids were thoroughly stirred for 1 h to obtain an organic solvent for mixing fluorescent glass. Finally, the mixture with different refractive indexes was brushed on the quartz glass through screen printing in the order from small to large refractive index films to prepare the gradient-refractive phosphor-in-glass (PIG) coating.

Samples were characterized by the X-ray diffractometer (XRD 6100, SHIMADZU, Nanjing, China), and radiation was applied at 40 kV and 40 mA, ranging from 10° to 80° . The fluorescence spectrum of the sample was measured by a fluorescence spectrophotometer (Acton spectra pro sp-2300). The transmittance of glass and the absorption value of fluorescent glass were tested by a UV-visible diffuse reflectance spectrum (UV-3600).

3. Results and Discussion

3.1. Spectral Properties of Fluorescent Powder

The luminescence pictures of the SLSO: $\text{Mn}^{4+}, \text{Mg}^{2+}$ phosphors excited by the natural light and a 365 nm NUV lamp are shown in Figure 1. Pure SLSO phosphor does not emit light under the excitation of the natural and 365 nm light, as shown in Figure 1a. It shows that pure SLSO is not excited at 365 nm. Comparing Figure 1b with Figure 1c, it shows that with the addition of Mn^{4+} ions, SLSO emits red light, meaning that the luminescence density will be quenched with the excess of Mn^{4+} [22].

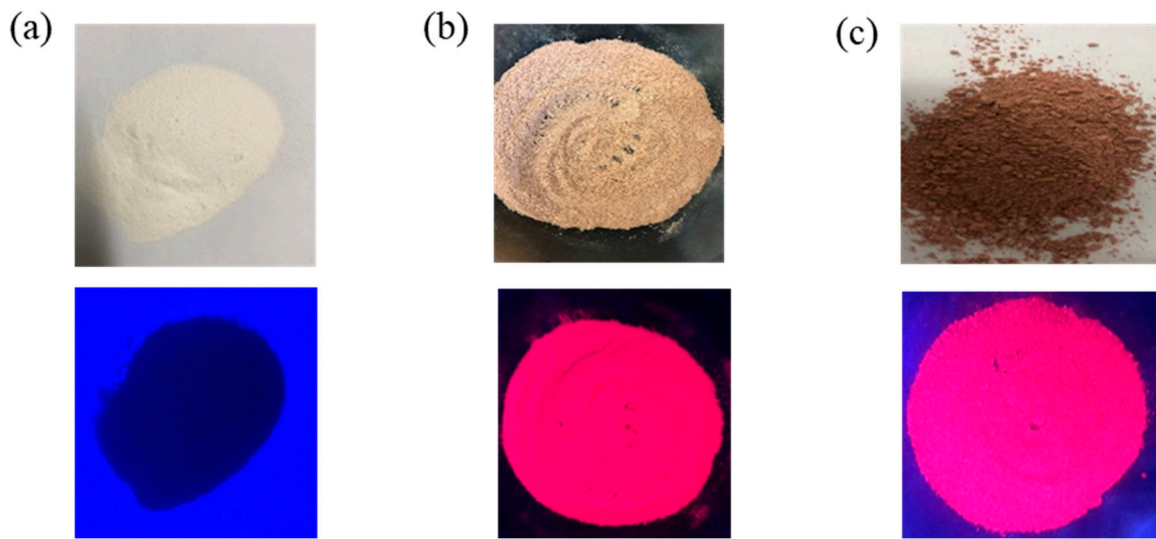


Figure 1. The luminescence pictures of (a) SLSO, (b) SLSO: 0.2%Mn⁴⁺, 0.3%Mg²⁺ phosphor, and (c) SLSO: 2%Mn⁴⁺, 3%Mg²⁺ phosphors under natural light (**top**) and 365 nm NUV lamp (**bottom**).

The SLSO crystal belonged to the characteristic double-perovskite family [23]. Considering effective ionic radius with different coordination numbers (CN), the Mn⁴⁺ ($r = 0.53 \text{ \AA}$, CN = 6) ions are expected to occupy the Sb⁵⁺ ($r = 0.6 \text{ \AA}$, CN = 6) site [24]. The Mg²⁺ ions ($r = 0.72 \text{ \AA}$, CN = 6) and Li⁺ ions ($r = 0.76 \text{ \AA}$, CN = 6) are relatively close, so the Mg²⁺ ions might substitute for Li⁺ sites or occupy Li⁺ vacancies, and then compensate for the imbalanced charges in SLSO phosphors [25]. Because of the charge compensation, the formation of the defects which served as quenching centers in the SLSO phosphors was avoided [26]. Therefore, the luminous intensity and internal quantum efficiency (IQE) of SLSO: 0.2%Mn⁴⁺, 0.3% Mg²⁺ phosphors were greatly improved.

The XRD of Mn⁴⁺ and Mg²⁺ co-doped SLSO, pure SLSO samples and SLSO standard comparison cards were shown in Figure 2a. All diffraction peaks are similar to SLSO standard data in Document JCPDS No. 51-1774 [27]. It can be observed that no additional diffraction peaks were found, indicating that all samples were successfully synthesized. The XRD diffraction peak is very sharp, indicating that the phosphor sample has excellent crystallization performance. Figure 2b shows the magnification of the main diffraction peaks (about 26.4°). With the addition of Mn⁴⁺ ions, the position of the diffraction peak had shifted a little, suggesting a shrinkage of the crystal lattice by Mn⁴⁺ doping.

The photoluminescence (PL) spectra and luminescence picture of SLSO: 0.2%Mn⁴⁺, 0.3% Mg²⁺ phosphor under 365 nm excitation were shown in Figure 3a. Upon the excitation at 365 nm, it can be found that the phosphor emits wide far-red light peaking at 692 nm, which is owing to ²E_g to ⁴A_{2g} of the Mn⁴⁺ spin forbidden transition. Figure 3b shows the PL spectra of SLSO: 0.2%Mn⁴⁺, 0.3%Mg²⁺ phosphor and the absorption of PR and PFR. The emission peak of phosphor overlaps with the absorption peak of PFR, which means that the far-red light from the SLSO: Mn⁴⁺, Mg²⁺ can be absorbed by PFR and converted into PR, thus promoting the growth of plants. The internal quantum efficiency (IQE) was calculated by the following equation [28]:

$$IQE = \frac{\text{Number of photons as PL from sample}}{\text{Number of photons absorbed by sample}} \quad (1)$$

Under 365 nm excitation, the emission spectrum shows a wide band with 692 nm as the center in the 550–800 nm range, and its IQE is 86.67%. In addition, there is a significant overlap between PFR and Mn⁴⁺ emission. Therefore, SLSO: Mn⁴⁺, Mg²⁺ phosphors show potential in plant LED, which is essential for plant growth.

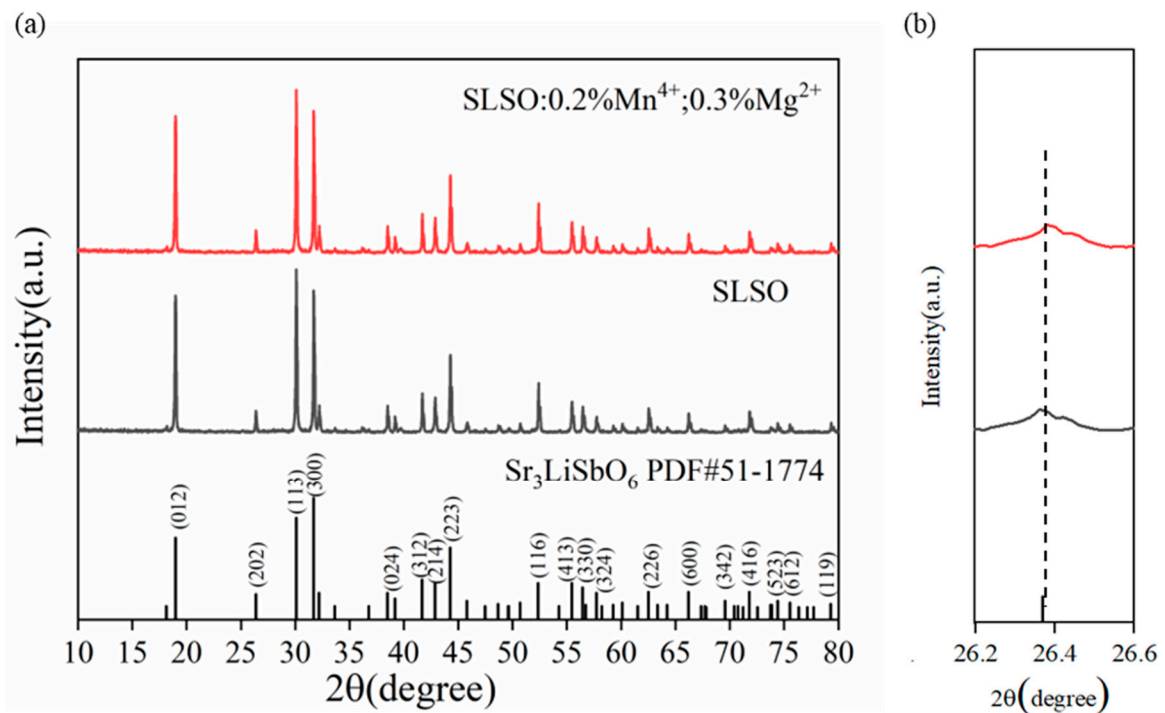


Figure 2. (a) XRD patterns of Mn^{4+} and Mg^{2+} co-doped SLSO, pure SLSO samples and SLSO standard comparison cards. (b) the magnified XRD curves range from 26.2° to 26.6° .

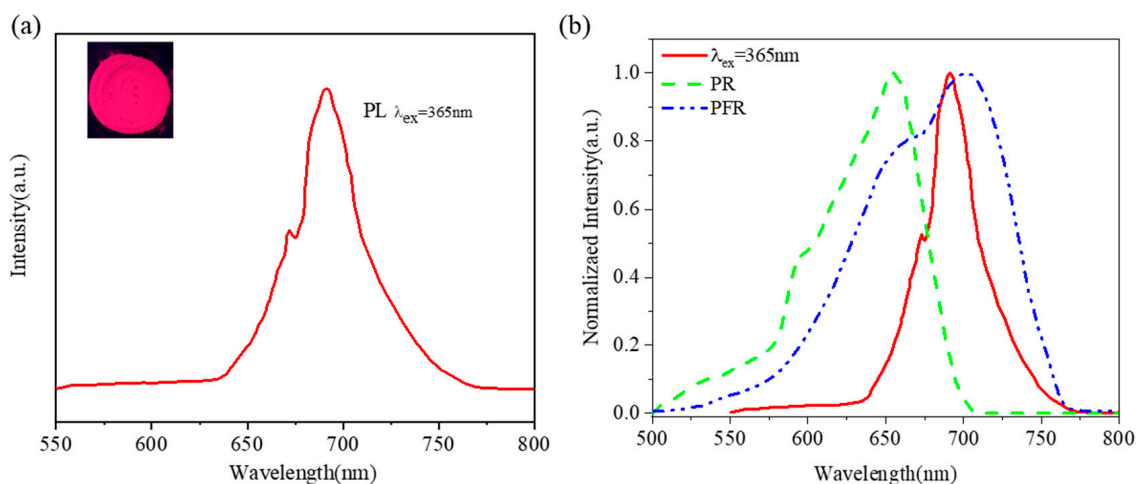


Figure 3. (a) PL spectrum of SLSO: 0.2% Mn^{4+} , 0.3% Mg^{2+} phosphor at 365 nm, (b) PR and PFR in plants and PL spectra of SLSO: 0.2% Mn^{4+} , 0.3% Mg^{2+} phosphors.

3.2. Spectral Property of Refractive Glass

The refractive indexes of P_2O_5 - ZnO - B_2O_3 - Li_2CO_3 - BaO glass were adjusted by changing the BaO concentration. With the increase in BaO, the value of refractive index changes from 1.6215 to 1.7635. The reason for using 3%, 6%, and 9% BaO concentrations in the three-layer glass is to ensure that the difference in refractive indices between the layers remains consistent, resulting in a smoother and more gradual refractive index change.

As shown in Figure 4a, the P_2O_5 - ZnO - B_2O_3 - Li_2CO_3 - BaO glass has high transparency and good transmittance in visible light. The insets are actual images of the glass, demonstrating its characteristic of being colorless and transparent. The effect of BaO concentration on the refractive index in matrix glass was displayed in Figure 4b. Due to the higher density of Ba^{2+} and the increase in electron polarization time, the refractive index of glass increases gradually with the increase in BaO [29]. The longer the polarization time is, the

higher the refractive index will be. Compared with other raw materials, BaO has a higher molecular weight. The higher the BaO concentration of the matrix glass, the higher the refractive index. This kind of glass sample is of great significance to the study of graded index fluorescent glass. The absorption spectrum of the P_2O_5 -ZnO- B_2O_3 - Li_2CO_3 -BaO glass sample at 300 nm~800 nm is shown in Figure 4b. It was found that the absorptivity of glass increases with the increase in barium content, and 3% BaO glass has the lowest absorption rate, while 9% BaO glass has the highest absorption rate. We also found that the absorption of the glass sample is mainly concentrated around 345 nm, and the absorption at 365 nm is less, which can be well applied to the fluorescent glass packaged NUV-LED.

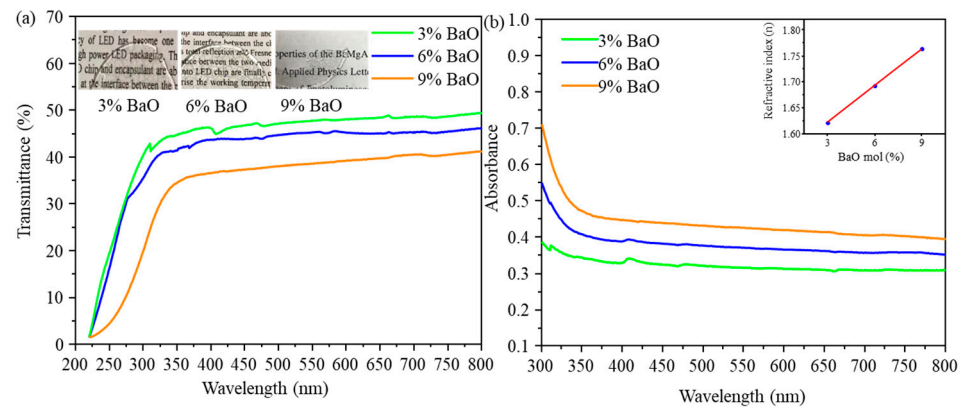


Figure 4. (a) The transmittance spectra of P_2O_5 -ZnO- B_2O_3 - Li_2CO_3 -xBaO (x = 3, 6, 9%) glass, (b) The absorption spectra of P_2O_5 -ZnO- B_2O_3 - Li_2CO_3 -xBaO (x = 3, 6, 9%) glass.

3.3. Light-Transmission Process in Gradient Index Fluorescent Glass

Using Monte Carlo simulation [30], the movement of photons in gradient refraction glass is simulated and we studied the concentration of phosphor dependent on the luminous efficiency and the transmittance of ultraviolet and far-red light. Figure 5 shows the light-transmission process in gradient index fluorescent glass, in which Fresnel reflection occurs between different refractive indexes. The purple line indicates the light emitted from the LED Chip, and the red dotted line represents the light emitted by the excited Fluorescent particles. In this figure, we illustrate the process of photon transport within the fluorescent glass, which involves interactions between randomly generated excitation photons and fluorescent particles (phosphors) in the glass. Snell's Law [31] is:

$$n_1 \sin \theta_1 = n_2 \sin \theta_2 \quad (2)$$

where θ_1 is the incident angle, θ_2 is the transmission angle, and n_1 and n_2 are the refractive indexes, if $\theta_2 = 90^\circ$, total reflection actually occurs. The smaller the difference between n_1 and n_2 , the greater the light output. The internal refractive index of the NUV chip is fixed at 2.5, and the refractive index of the air is 1. The smaller the refractive index difference is, the smaller the internal reflection loss is, which increased the number of photons at the exit boundary and improved the light output efficiency of LED. Therefore, gradient refraction is conducive to optical output and has better optical output efficiency.

In the actual fluorescent glass, the photon movement process is quite complex. To simplify the computation, the following assumptions are made when using the Monte Carlo simulation method [32]:

- (1) The properties of photons are assumed to be stable. The parameters obtained for photons remain constant, and variations in wavelength and frequency are not considered.
- (2) Photon polarization phenomena are ignored, and the movement direction of the photons is considered to be in a straight line.
- (3) Effects of bubbles, impurities, and cracks on the scattering, absorption, and transmission of photons are ignored, assuming that there are no impurities in the medium.

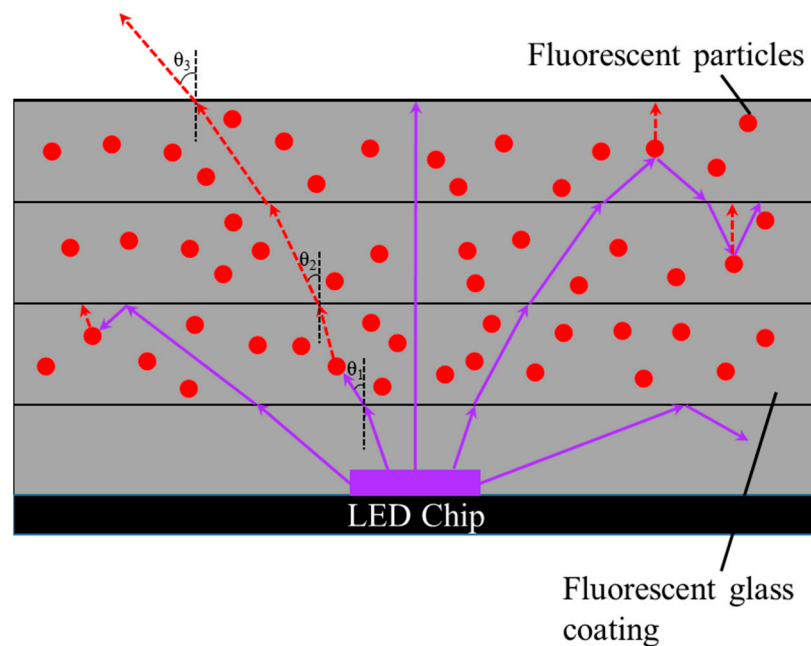


Figure 5. Light-transmission process in gradient index fluorescent glass.

The present study developed a simulation program based on the Monte Carlo method using MATLAB software. The emission direction of the photons was determined by random numbers. To simplify the simulation process and speed up computation, this study utilized a packet of photons with a weighted value to replace single photon simulations, following the methodology outlined in reference [32]. The initial weight was set at 1. As the photon packet moves within the fluorescent glass, it splits into smaller packets, while simultaneously generating new photon packets that require a reevaluation of their weight. The sum of the weight of these photon packets should not exceed the initial weight. When a photon packet reaches the boundary, it is divided into scattered photon packets and escaped photon packets, each assigned different weights. The parameters of the escaped photon packets serve as the final output values for the fluorescent glass. To reduce the computational load, a roulette wheel selection method was implemented for the energy transfer of low-weight photon packets. Photon packets with weights below 0.001 were set and were removed via roulette wheel selection. According to probability theory, the weight of the photon packet decreases during its motion, tending asymptotically to zero. However, for photon packets with small weights, the energy value has a very limited and negligible impact on the final statistical results. The process of photon transmission simulation is depicted in Figure 6, as described in reference [32].

In the simulation of the emission of Mn^{4+} -doped far-red LED, the plane size of the fluorescent glass is set to $1\text{ mm} \times 1\text{ mm}$. The incident wavelength is set to 365 nm, the phosphor excitation wavelength to 692 nm, and the scattering absorption coefficients for ultraviolet and far-red light are set to 5.34 mm^{-1} and 3.18 mm^{-1} , and 6.34 mm^{-1} and 0.0233 mm^{-1} , respectively. The anisotropic parameter of the phosphor silicone gel is $g = 0.8$, the refractive index is n , and the quantum efficiency $\eta = 0.9$. Ultraviolet light transmittance represents the amount of ultraviolet light transmitted at the upper boundary of the phosphate fluorescent glass film, red-light transmittance represents the amount of red light passing through the upper boundary of the phosphate fluorescent glass film, and red-light reflectance represents the amount of red light passing through the lower boundary of the phosphate fluorescent glass film. Figure 7 shows the effects of different phosphor concentrations and thicknesses, as well as gradient-refractive index packaging LEDs (with a refractive index n of 1.763, 1.692, 1.621) on UV transmission, red-light transmission, and red-light reflection.

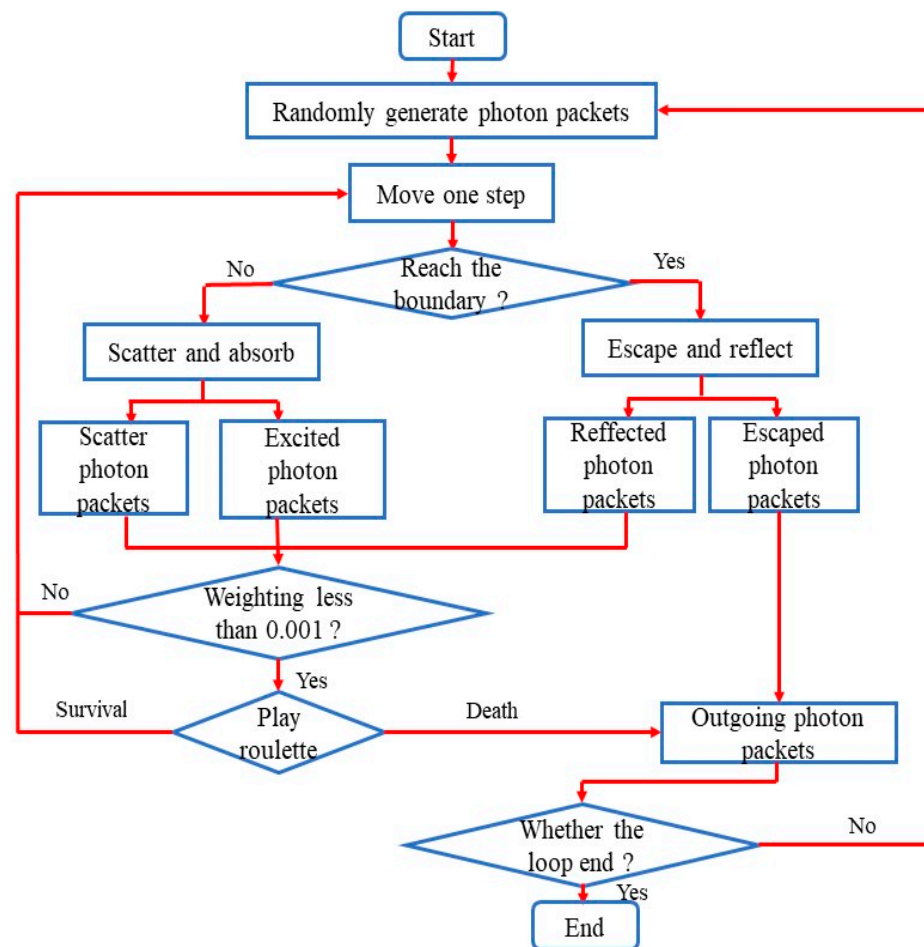


Figure 6. Monte Carlo simulation flow chart [32].

Figure 7a shows the trend of UV transmittance of the fluorescent glass with changes in the concentration and thickness of fluorescent particles. As the concentration and thickness of the fluorescent glass increase, the UV light transmittance decreases exponentially. This is due to an increase in the number of fluorescent particles, leading to an increase in the absorption ratio of UV light particles. When the thickness of the fluorescent glass and the concentration of the phosphor are greater than 0.15 mm and 1.1 g/cm³, respectively, the UV light output rate is less than 40%, and the change tends to be flat. Therefore, it is necessary to control the UV luminous efficiency within the range of 40–60%. Figure 7b shows that with the increase in the concentration and thickness of red fluorescent particles and glass, the far-red-light transmittance first increases and then decreases. This is due to the rapid increase in the probability of UV light absorption leading to a significant increase in the excitation probability of phosphor particles and a rapid increase in the number of far-red-light photons. However, as the absorption and excitation capability of the phosphor gradually saturates, the transmittance of far-red light reaches a peak. Increasing the concentration and thickness of the fluorescent glass will increase the probability of scattering far-red light in the fluorescent glass. The increase in light energy loss and backward-scattering effect leads to a reduction in far-red-light transmittance. From the results, when the thickness of the fluorescent glass is greater than 0.15 mm, the peak values of far-red light are concentrated at a concentration of 0.4–0.6 g/cm³. In Figure 7c, the far-red-light loss rate exponentially increases with the increase in the concentration and thickness of phosphor, indicating that the fluorescent glass has a strong backward-scattering effect. When the concentration is stable at more than 0.9 g/cm³, the backward reflectance of the far-red light in the fluorescent glass is as high as 11.3%, and it tends to be stable when the phosphor concentration is greater than 0.6 g/cm³. It is evident that the concentration of

phosphor and the thickness of the structure have a significant impact on the light efficiency of fluorescent glass. Combining theory with experiment, it is decided that during the LED packaging process, the thickness of the fluorescent glass is chosen to be 0.15 mm and the concentration of the phosphor is chosen to be 0.6 g/cm³.

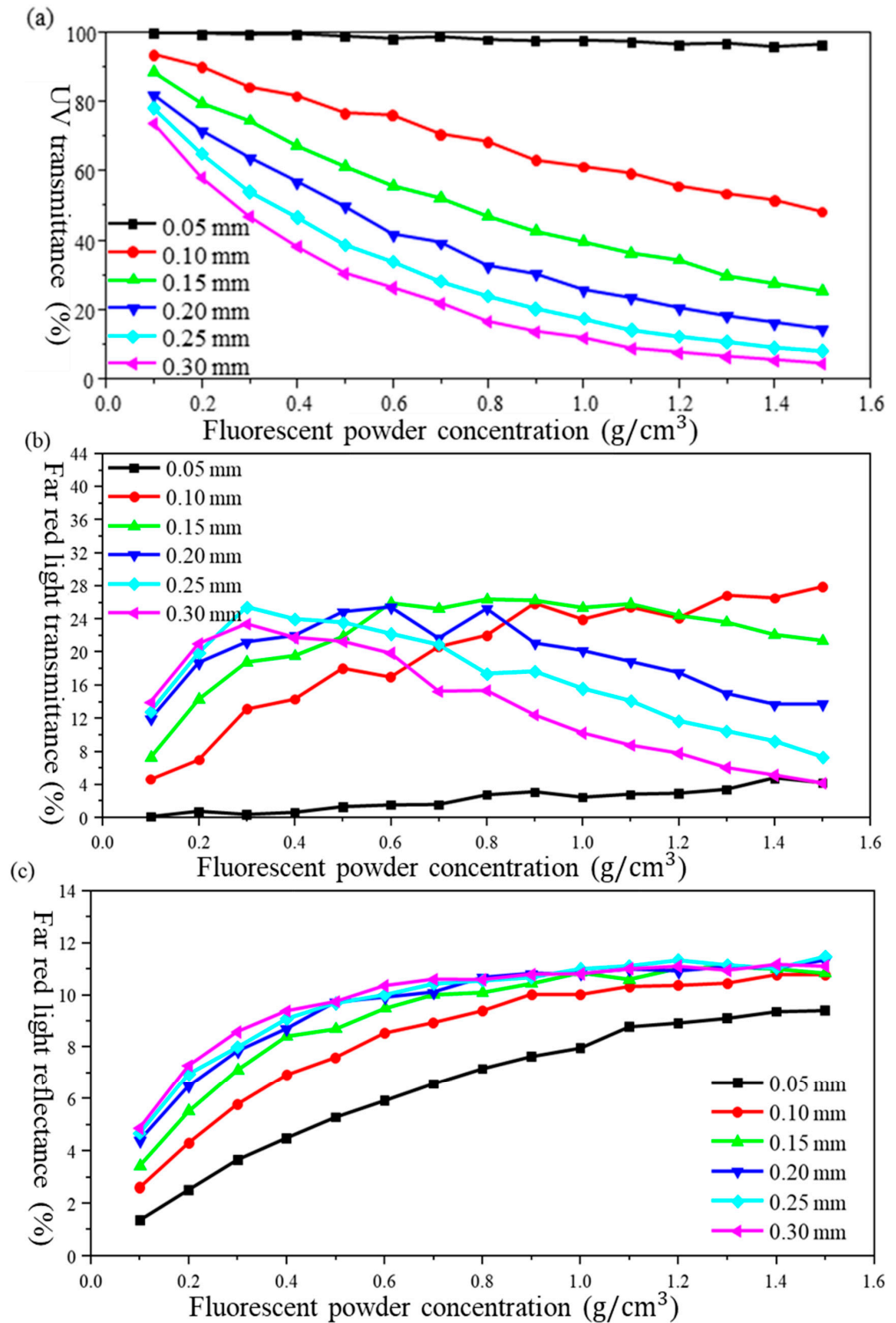


Figure 7. The (a) UV light transmittance, (b) far-red-light transmittance, and (c) far-red-light reflectance of the LED encapsulated with Mn⁴⁺-doped PIG film.

3.4. Spectral Properties of Gradient Refractive Glass Encapsulated LED

The pictures of fluorescent glass excited by the 365 nm LED chip and the absorption value of 320~1000 nm fluorescent glass are shown in Figure 8a. Due to the mixing of glass and phosphor, the absorption value of phosphor will also affect the overall structure. The fluorescent glass coating has obvious absorption to 365 nm wavelength. As the number of layers increases, red-light conversion efficiency and LED light output efficiency also change significantly. As shown in Figure 8b, the package-layer-dependent emission intensity of LEDs under 365 nm excitation. It shows that the LED encapsulated by the three-layer gradient-refractive glass has the strongest red intensity emission, which is significantly higher than other samples. The IQE of this LED was 93.6%.

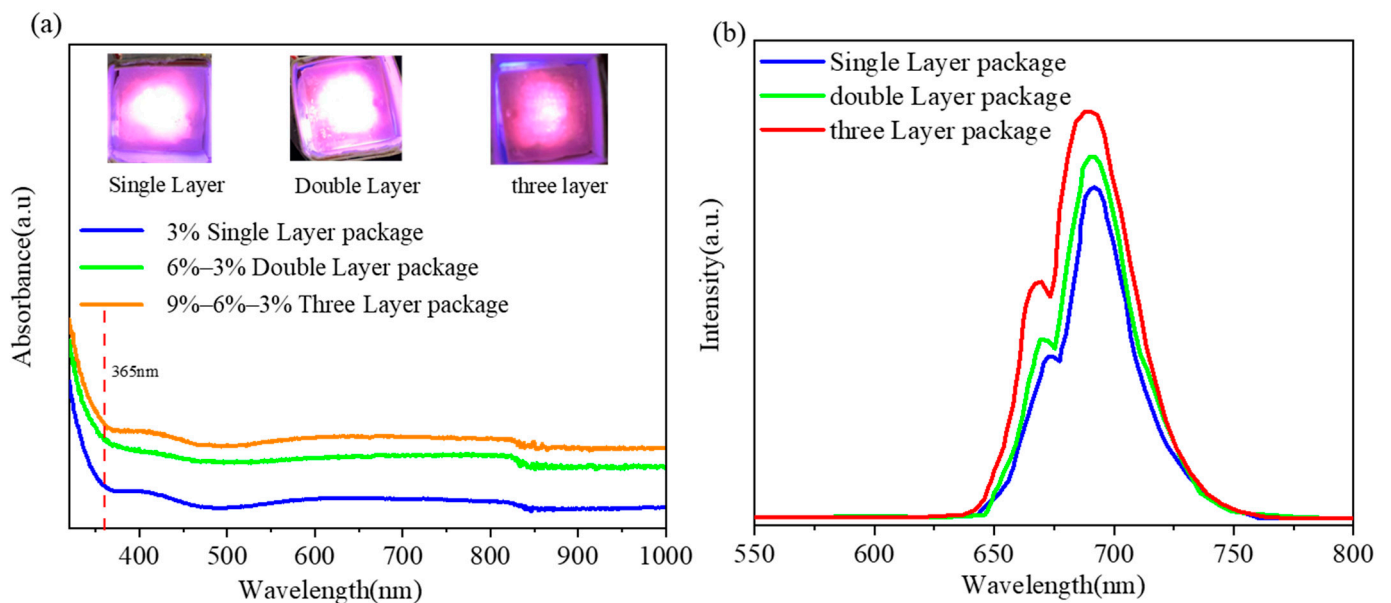


Figure 8. (a) Absorption spectra of multi-layer PIG packaged LED. (b) The package layer-dependent emission intensity of LEDs under 365 nm excitation.

Figure 9 displays the color coordinates and color temperature of the phosphor and gradient-refraction packaged LED under the excitation of 365 nm. The excitation wavelength of 365 nm, within the ultraviolet light range, was selected as it effectively excites the phosphor to emit visible light, a common excitation method for phosphors. Under phosphor, the fluorescent pink coordinates are $x = 0.7258$, $y = 0.2735$, and the color coordinates for the gradient refraction packaged LED are $x = 0.3385$, $y = 0.3431$, with a color temperature of 5235 K. The luminous efficacy of the traditional (SI) LED, without gradient refraction, is 59 lm/W. As illustrated in Table 1, the luminous efficacies of PIG 9-6-3, PIG-9-9-9, PIG-6-6-6, and PIG-3-3-3 are 96.74 lm/W, 63.39 lm/W, 65.31 lm/W, and 68.75 lm/W, respectively. This represents an increase of 62.7% in the luminous efficacy of the new LED, demonstrating that the gradient index packaged structure has a positive impact on improving light output efficiency. The gradient refraction rate indeed has an inherent advantage in reducing reflective losses and increasing the number of photons at the exit boundary, contributing to the enhancement of LED light output efficiency. Different PIGs may have varied effects on luminous efficiency. For instance, PIG 9-6-3 displays the highest luminous efficiency, possibly attributed to its internal structure and phosphor material characteristics. Furthermore, the color temperatures (CCT) of these samples were 5235 K, 5289 K, 5204 K, and 5228 K, respectively, as described in Table 1. These color temperatures are close to white light (5200 K), suggesting that Mn^{4+} is a promising candidate to replace Ce^{2+} in LED packaging. This is due to the fact that the color temperature range for white light is typically considered to be 5000–6000 K, and a color temperature close to white light provides a more comfortable light color, meeting the needs of everyday illumination.

The emission wavelength of Mn^{4+} is primarily concentrated in the red- and far-red-light areas, which are essential for plant growth, implying a promising application prospect for Mn^{4+} in the LED plant growth lighting sector. In conclusion, fluorescent glass with a gradient index demonstrates substantial advantages in improving luminous efficiency when packaging LEDs.

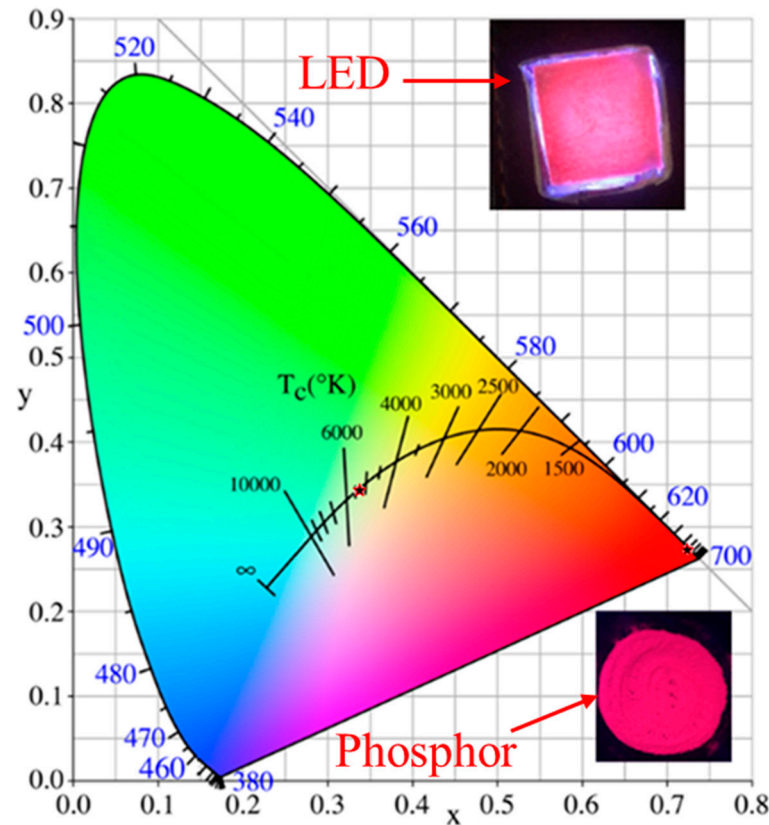


Figure 9. The color coordinates and color temperature of phosphor and gradient refraction packaged LEDs under 365 nm excitation.

Table 1. Color coordinates, color rendering index, color temperature, and luminous efficiency of different LEDs.

Sample	CIE (x)	CIE (y)	CCT (K)	Luminous Efficiency (lm/W)
PIG-9-6-3	x = 0.3385	y = 0.3431	5235	96.74
PIG-9-9-9	x = 0.3375	y = 0.3389	5289	63.39
PIG-6-6-6	x = 0.3389	y = 0.3468	5204	65.31
PIG-3-3-3	x = 0.3388	y = 0.3452	5228	68.75
SI	x = 0.3299	y = 0.3186	5605	59

4. Conclusions

Compared with traditional packages, gradient-refractive fluorescent glass packages have higher luminous efficiency. Mn^{4+} and Mg^{2+} co-doped Sr_3LiSbO_6 have red and far-red light consistent with plant growth. With the increase in BaO concentration, the refractive index of the matrix glass increases from 1.62 to 1.76. With the addition of a gradient refraction glass package, the IQE of the resulting LED was 93.6%. The luminous efficacy of traditional LED and gradient-refracted fluorescent glass encapsulated LED were 59 lm/W and 96.74 lm/W, which has improved by 62.7%. The results show that the gradient-refraction fluorescent glass coating is beneficial in improving the luminous efficacy of LED.

With the improvement of luminous efficacy, the photosynthetic effective radiation of plants also increases correspondingly. It has been proven that the gradient refraction coating has great potential in packaged LED applications and has a good application prospect in plant light filling.

Author Contributions: Methodology, X.W.; Data curation, B.W.; Writing—original draft, S.L.; Funding acquisition, X.Y. All authors have read and agreed to the published version of the manuscript.

Funding: This work was supported by the State Key Laboratory of Refractories and Metallurgy (Wuhan University of Science and Technology) (G202302), Natural Science Foundation of Jiangsu Higher Education Institutions of China (Grant No. 23KJA510005). Additional funding was provided by Professor Xiangfu Wang from Nanjing University of Posts and Telecommunications, with a total of 1 sponsor.

Data Availability Statement: No new data were created or analyzed in this study. Data sharing is not applicable to this article as no datasets were generated or analyzed during the current study.

Conflicts of Interest: The authors declare no conflict of interest.

References

1. Huang, X.; Li, B.; Guo, H.; Chen, D. Molybdenum-doping-induced photoluminescence enhancement in Eu^{3+} -activated CaWO_4 red-emitting phosphors for white light-emitting diodes. *Dyes Pigm.* **2017**, *143*, 86. [CrossRef]
2. Mao, Z.; Chen, J.; Jian, L.; Wang, D. Dual-responsive $\text{Sr}_2\text{SiO}_4:\text{Eu}^{2+}-\text{Ba}_3\text{MgSi}_2\text{O}_8:\text{Eu}^{2+}, \text{Mn}^{2+}$ composite phosphor to human eyes and plant chlorophylls applications for general lighting and plant lighting. *Chem. Eng. J.* **2016**, *284*, 1003. [CrossRef]
3. Li, L.; Pan, Y.; Chen, Z.; Huang, S.; Wu, M. Tunable luminescence and energy transfer properties of Bi^{3+} and Mn^{4+} co-doped $\text{Ca}_{14}\text{Al}_{10}\text{Zn}_6\text{O}_{35}$ phosphors for agricultural applications. *RSC Adv.* **2017**, *7*, 14868. [CrossRef]
4. Zheng, Y.; Zhang, H.; Zhang, H.; Xia, Z.; Liu, Y.; Molokeev, M.; Lei, B. Co-substitution in $\text{Ca}_{1-x}\text{Y}_x\text{Al}_{12-x}\text{Mg}_x\text{O}_{19}$ phosphors: Local structure evolution, Photoluminescence tuning and application for plant growth LEDs. *J. Mater. Chem. C* **2018**, *6*, 4217. [CrossRef]
5. Legendre, R.; van Iersel, M.W. Supplemental far-red light stimulates lettuce growth: Disentangling morphological and physiological effects. *Plants* **2021**, *10*, 166. [CrossRef]
6. Li, Y.; Liu, Z.; Shi, Q.; Yang, F.; Wei, M. Mixed red and blue light promotes tomato seedlings growth by influencing leaf anatomy, photosynthesis, CO_2 assimilation and endogenous hormones. *Sci. Hort.* **2021**, *290*, 110500. [CrossRef]
7. Jin, W.; Urbina, J.L.; Heuvelink, E.; Marcelis, L.F. Adding far-red to red-blue light-emitting diode light promotes yield of lettuce at different planting densities. *Front. Plant. Sci.* **2021**, *11*, 609977. [CrossRef]
8. Kusuma, P.; Bugbee, B.J. Far-red fraction: An improved metric for characterizing phytochrome effects on morphology. *Am. Soc. Hort. Sci.* **2021**, *146*, 3. [CrossRef]
9. Pust, P.; Schmidt, P.J.; Schnick, W. A revolution in lighting. *Nat. Mater.* **2015**, *14*, 454. [CrossRef]
10. Lin, C.C.; Liu, R.S. Advances in phosphors for light-emitting diodes. *J. Phys. Chem. Lett.* **2011**, *2*, 1268. [CrossRef]
11. Zhu, H.; Lin, C.C.; Luo, W.; Shu, S.; Liu, Z.; Liu, Y.; Kong, J.; Ma, E.; Cao, Y.; Liu, R.S.; et al. Highly efficient non-rare-earth red emitting phosphor for warm whitelight-emitting diodes. *Nat. Commun.* **2014**, *5*, 4312. [CrossRef]
12. Danziger, N.; Bernstein, N. Light matters: Effect of light spectra on cannabinoid profile and plant development of medical cannabis (*Cannabis sativa* L.). *Ind. Crops Prod.* **2021**, *164*, 113351. [CrossRef]
13. Pan, Z.; Zeng, K.; Huang, B.; Zhu, L.J. Synthesis of hydrogen-containing methyl phenyl silicone resins with a high refractive index for LED Encapsulation. *Electron. Mater.* **2020**, *49*, 4816. [CrossRef]
14. Liu, E.; Hanss, A.; Schmid, M.; Elger, G. The influence of the phosphor layer as heat source and up-stream thermal masses on the thermal characterization by transient thermal analysis of modern wafer level high power LEDs. *Microelectron. Reliab.* **2016**, *67*, 29. [CrossRef]
15. Zhu, Y.; Hu, J.; Hu, R.; Duan, B.; Luo, X. Thermal model of phosphor self-heating in phosphor-converted light-emitting diodes. *ICEPT* **2015**, *16*, 1090.
16. Li, J.S.; Yan, C.M.; Li, Z.T.; Liang, G.W.; Tang, Y.; Yu, B.H. Color Uniformity Enhancement for WLEDs Using Inverted Dispensing Method. *IEEE Photonic Technol. Lett.* **2017**, *29*, 2079. [CrossRef]
17. Ahn, S.H.; Nam, Y.H.; Han, K.; Im, W.B.; Cho, K.Y.; Chung, W.J. Phosphor-in-glass thick film formation with low sintering temperature phosphosilicate glass for robust white LED. *J. Am. Ceram. Soc.* **2017**, *100*, 1280. [CrossRef]
18. Huang, P.; Luo, P.; Zhou, B.; Wang, L.; Jiang, W. Preparation and luminescence of transparent silica glass-ceramics containing $\text{LaF}_3:\text{Eu}^{3+}$ nanocrystals. *Mater. Lett.* **2020**, *271*, 127764. [CrossRef]
19. Peng, Y.; Li, R.; Cheng, H.; Chen, Z.; Li, H.; Chen, M. Facile preparation of patterned phosphor-in-glass with excellent luminous properties through screen-printing for high-power white light-emitting diodes. *J. Alloys Compd.* **2017**, *693*, 279. [CrossRef]
20. Cao, R.; Wu, L.; Di, X.; Li, P.; Hu, G.; Liang, X.; Xiang, W. A WLED based on $\text{LuAG}:\text{Ce}^{3+}$ PiG coated red-emitting $\text{K}_2\text{SiF}_6:\text{Mn}^{4+}$ phosphor by screen-printing. *Opt. Mater.* **2017**, *70*, 92. [CrossRef]

21. Kim, L.; Shin, M.W. Thermal resistance measurement of LED package with multichips. *IEEE Trans. Comp. Packag. Technol.* **2007**, *30*, 632.
22. Cao, R.; Zhang, F.; Xiao, H.; Chen, T.; Guo, S.; Zheng, G.; Yu, X.; Chen, T. Perovskite La_2LiRO_6 : Mn^{4+} (R = Nb, Ta, Sb) Phosphors: Synthesis and Luminescence Properties. *Inorg. Chim. Acta* **2018**, *483*, 593. [[CrossRef](#)]
23. Fu, L.; Yang, Y.; Zhang, Y.; Ren, X.; Zhu, Y.; Zhu, J.; Wu, Y.; Wang, J.; Feng, X. The novel $\text{Sr}_3\text{LiSbO}_6$: Mn^{4+} , Ca^{2+} far-red-emitting phosphors with over 95% internal quantum efficiency for indoor plant growth LEDs. *J. Lumin.* **2021**, *237*, 118165. [[CrossRef](#)]
24. Wang, L.; Yuan, L.; Xu, Y.; Zhou, R.; Qu, B.; Ding, N.; Shi, M.; Zhang, B.; Chen, Y.; Jiang, Y.; et al. Luminescent properties of $\text{La}_2\text{LiTaO}_6$: Mn^{4+} and its application as red emission LEDs phosphor. *Appl. Phys. A* **2014**, *117*, 1777. [[CrossRef](#)]
25. Ren, X.; Zhang, Y.; Su, C.; Zhan, J.; Fu, L.; Yang, Y.; Sun, X.; Wang, J.; Feng, X. High quantum efficiency and luminescence properties of far-red $\text{Sr}_3\text{NaTaO}_6$: Mn^{4+} , Ba^{2+} phosphor for application in plant growth lighting LEDs. *J. Lumin.* **2022**, *244*, 118701. [[CrossRef](#)]
26. Zhong, J.; Chen, D.; Chen, X.; Wang, K.; Li, X.; Zhu, Y.; Jia, Z. Efficient rare-earth free red-emitting Ca_2YSbO_6 : Mn^{4+} ,M (M = Li^+ , Na^+ , K^+ , Mg^{2+}) phosphors for white light-emitting diodes. *Dalton Trans.* **2018**, *47*, 6528. [[CrossRef](#)]
27. Shi, L.; Han, Y.; Zhao, Y.; Li, M.; Geng, X.; Zhang, Z.; Wang, L. Synthesis and photoluminescence properties of novel $\text{Sr}_3\text{LiSbO}_6$: Mn^{4+} red phosphor for indoor plant growth. *Opt. Mater.* **2019**, *89*, 609. [[CrossRef](#)]
28. Li, Y.; Yin, Y.; Wang, T.; Wu, J.; Zhang, J.; Yu, S.; Zhang, M.; Zhao, L.; Wang, W. Ultra-bright green-emitting phosphors with an internal quantum efficiency of over 90% for high-quality WLEDs. *Dalton Trans.* **2021**, *50*, 4159. [[CrossRef](#)] [[PubMed](#)]
29. Fantone, S.D. Refractive index and spectral models for gradient-index materials. *Appl. Opt.* **1983**, *22*, 432. [[CrossRef](#)]
30. Huang, Y.; Liang, X.G.; Xia, X.L. Monte Carlo simulation of radiative transfer in scattering, emitting, absorbing slab with gradient index. *J. Quant. Spectrosc. Radiat. Transf.* **2005**, *92*, 111. [[CrossRef](#)]
31. Wang, J.; Elghoul, G.; Peters, S. Lead zirconium titanate alternatives for nanoactuators. *IEEE Trans Ultrason Ferroelectr. Freq. Control.* **2013**, *60*, 256. [[CrossRef](#)] [[PubMed](#)]
32. Wang, B.; She, M.; Zhang, B.; Wang, X. Modeling and Monte Carlo simulation of photon transmission in glass-packaged WLEDs. *Displays* **2023**, *78*, 102431. [[CrossRef](#)]

Disclaimer/Publisher's Note: The statements, opinions and data contained in all publications are solely those of the individual author(s) and contributor(s) and not of MDPI and/or the editor(s). MDPI and/or the editor(s) disclaim responsibility for any injury to people or property resulting from any ideas, methods, instructions or products referred to in the content.